AMERICAN SOCIETY FOR MICROBIOLOGY | Molecular and Cellular Biology®

RESEARCH ARTICLE

DNA Damage Triggers the Nuclear Accumulation of RASSF6 Tumor Suppressor Protein via CDK9 and BAF53 To Regulate p53 Target Gene Transcription

Joshua Agbemefa Kuleape,[a] Shakhawoat Hossain,[a,b] Caleb Kwame Sinclear,[a] Takanobu Shimizu,[a] Hiroaki Iwasa,[a] Junichi Maruyama,[a] Kyoko Arimoto-Matsuzaki,[a] Hiroshi Nishina,[c] Yutaka Hata[a,d]

[a]Department of Medical Biochemistry, Graduate School of Medical and Dental Sciences, Tokyo Medical and Dental University, Tokyo, Japan
[b]Department of Biochemistry and Molecular Biology, University of Rajshahi, Rajshahi, Bangladesh
[c]Department of Developmental and Regenerative Biology, Medical Research Institute, Tokyo Medical and Dental University, Tokyo, Japan
[d]Center for Brain Integration Research, Tokyo Medical and Dental University, Tokyo, Japan

ABSTRACT RASSF6, a member of the tumor suppressor Ras-association domain family (RASSF) proteins, regulates cell cycle arrest and apoptosis via p53 and plays a tumor suppressor role. We previously reported that RASSF6 blocks MDM2-mediated p53 degradation and enhances p53 expression. In this study, we demonstrated that RASSF6 has nuclear localization and nuclear export signals and that DNA damage triggers the nuclear accumulation of RASSF6. We found that RASSF6 directly binds to BAF53, the component of SWI/SNF complex. DNA damage induces CDK9-mediated phosphorylation of BAF53, which enhances the interaction with RASSF6 and increases the amount of RASSF6 in the nucleus. Subsequently, RASSF6 augments the interaction between BAF53 and BAF60a, another component of the SWI/SNF complex, and further promotes the interaction of BAF53 and BAF60a with p53. *BAF53* silencing or *BAF60a* silencing attenuates RASSF6-mediated p53 target gene transcription and apoptosis. Thus, RASSF6 is involved in the regulation of DNA damage-induced complex formation, including BAF53, BAF60a, and p53.

KEYWORDS apoptosis, BAF53, BAF60a, CDK9, p53, RASSF6, signal transduction, tumor suppressor

Ras-association domain family 6 (RASSF6) is a member of the RASSF proteins (1–3). *RASSF6* is epigenetically silenced in various human cancers, and its low expression is associated with poor prognosis (4–13). RASSF6, when exogenously expressed, induces apoptosis and cell cycle arrest in various cells (1, 2, 14, 15). Conversely, RASSF6 depletion blocks DNA damage-induced cell cycle arrest and apoptosis, compromises DNA repair, and generates polyploid cells (16). Hence, RASSF6 is thought to be a tumor suppressor.

The most important mechanism underlying the tumor suppressor role of RASSF6 is p53 activation (16). DNA damage induced by VP-16 treatment or UV exposure and oncogenic stress caused by oncogenic RAS trigger p53-mediated gene transcription. Mechanistically, RASSF6 binds MDM2, blocks MDM2-mediated degradation, and increases p53 protein expression (16, 17). However, whether RASSF6 interacts with MDM2 in the cytoplasm or in the nucleus is not clear. In HEK293FT cells, exogenously expressed RASSF6 is mainly recovered in the nuclear fraction (16). In other cells, such as HCT116 cells, RASSF6 is detected mostly in the cytoplasm, while pRb recruits RASSF6 into the nucleus (18, 19). Notably, in p53-null H1299 cells, RASSF6 is localized in the cytoplasm and oncogenic RAS recruits MDM2 to the cytoplasm via RASSF6 (18). These findings prompted us to hypothesize that RASSF6 shuttles between the cytoplasm

Address correspondence to Shakhawoat Hossain, shossain@ru.ac.bd, or Yutaka Hata, yuhammch@tmd.ac.jp.

The authors declare no conflict of interest.

Received 25 June 2021
Returned for modification 10 August 2021
Accepted 6 December 2021

Accepted manuscript posted online 13 December 2021
Published 17 February 2022

and the nucleus and that a certain mechanism determines the balance in the subcellular distribution of RASSF6.

In this study, we first revealed that RASSF6 harbors a nuclear localization signal (NLS) and two nuclear export signals (NES). DNA damage increases the nuclear RASSF6. We found that RASSF6 interacts with the nuclear proteins, BAF53 and BAF60a. DNA damage enhances the interaction of RASSF6 with BAF53 and BAF60a. Therefore, we speculate that RASSF6 is trapped in the nucleus in response to DNA damage through the binding to BAF53 and BAF60a. We revealed that RASSF6 directly binds to BAF53 and that this interaction is enhanced by CDK9. Preceding studies reported that both BAF53 and BAF60a form a complex with p53 and regulate p53-mediated gene transcription (20–22). RASSF6 enhances the interaction of p53 with BAF53 and BAF60a, while *BAF53* silencing or *BAF60a* silencing attenuates RASSF6-induced p53 activation. These findings support the model that DNA damage activates p53 through RASSF6-BAF53-BAF60a axis, which is regulated by CDK9.

RESULTS

DNA damage induces the nuclear accumulation of RASSF6. We expressed green fluorescent protein (GFP)-RASSF6 in human colon cancer HCT116 cells and treated the cells with 50 μM VP-16. In the immunofluorescence, after 180 min, GFP-RASSF6 was accumulated in the nucleus (Fig. 1A). The increase of the nuclear RASSF6 was confirmed in the subcellular fractionation (Fig. 1B). We obtained similar results in human lung cancer H1299 cells (Fig. 1C and D). The nuclear accumulation of endogenous RASSF6 was observed in VP-16-treated SW480 cells (Fig. 1E and F). The exposure to UV also induced nuclear accumulation of RASSF6 (Fig. 1G and H). To determine which region of RASSF6 is involved in nuclear accumulation, we expressed GFP-tagged RASSF6 deletion constructs (Fig. 2A). VP-16 treatment induced the nuclear accumulation of GFP-RASSF6-N but not of GFP-RASSF6-del-N (Fig. 2B). RASSF6 harbors a putative NLS (LVRKRMKPL; single letters stand for amino acid residues) in the N-terminal region (Fig. 2A). An RASSF6 NLS mutant, in which RKR in NLS was mutated to AAA, did not enter the nucleus in response to DNA damage (Fig. 2C). RASSF6 also harbors two putative NES in the C-terminal region (NES1, LLESIL; NES2, IILKCL) (Fig. 2A). The RASSF6 NES1 mutant (LLESIL to RSESTL), NES2 mutant (IILKCL to TTRKCR), and NES1/2 mutant were distributed mostly in the nucleus even without VP-16 treatment (Fig. 2D). We also evaluated the effect of RASSF6 mutants on EdU incorporation. RASSF6 NES mutants, which were accumulated in the nucleus, blocked EdU incorporation, while the RASSF6-del-N or RASSF6 NLS mutant did not, which suggests that the nuclear RASSF6 induces cell cycle arrest, whereas the cytoplasmic RASSF6 does not (Fig. 3). Moreover, it is likely that RASSF6 shuttles between the cytoplasm and the nucleus and that DNA damage may increase the nuclear incorporation or decrease the nuclear export of RASSF6.

ATM or ATR is not involved in the DNA damage-induced nuclear accumulation of RASSF6. We attempted to identify the molecular mechanism underlying the DNA damage-induced nuclear accumulation of RASSF6. As DNA damage triggers the nuclear accumulation, we speculated that ATM, ATR, DNA-PK, or JNK may herein play a role. Therefore, we examined the effect of kinase inhibitors, 10 μM KU-55933 and 10 μM AZ20. Although the inhibition of ATM or ATR itself may compromise DNA repair and induce cell cycle defect, KU-55933 or AZ20 did not block the nuclear accumulation of RASSF6 (data not shown). Likewise, neither 10 μM NU7441 nor 10 μM SP600125 had any effect. We also tested imatinib, 1 μM saracatinib, 50 μM BAPTA-AM, 0.5 μM latrunculin A, 0.1 μM cytochalasin D, and 10 μM Y27632, none of which showed any effect (data not shown).

BAF60a is involved in the DNA damage-induced nuclear accumulation of RASSF6. We next hypothesized that RASSF6 may be trapped in the nucleus through interacting with certain nuclear proteins in response to DNA damage. As RASSF6 directly binds to MDM2 and indirectly interacts with p53, we first examined whether MDM2 or p53 is required for the nuclear accumulation of RASSF6. VP-16 treatment induced the nuclear accumulation of RASSF6 even after *MDM2* silencing or *TP53*

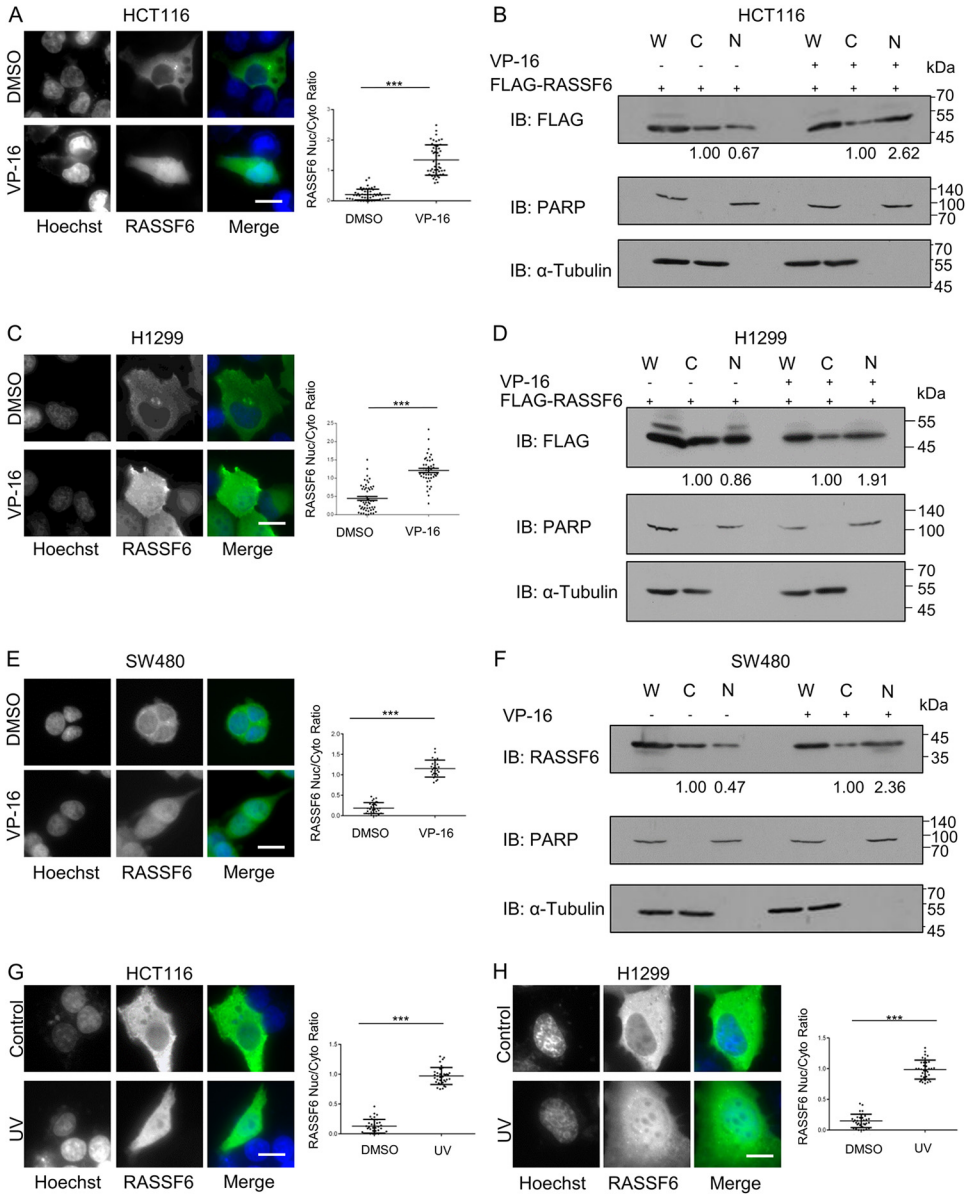

FIG 1 DNA damage induces the nuclear accumulation of RASSF6. (A, C, G, H) GFP-RASSF6 was expressed in human colon cancer HCT116 or human lung cancer H1299 cells. Twenty-four hours after transfection, cells were exposed to 50 μM VP-16 for 180 min in panels A and C and to 25 J/m^2 of UV radiation in panels G and H. The cells were fixed 180 min later. Nuclei were visualized with Hoechst 33342. Scale bars, 25 μm. The distributions of RASSF6 in the nucleus and the cytoplasm were measured by ArrayScan in 50 cells. ***, $P < 0.001$. (B, D) Subcellular fractionation was performed. The samples were immunoblotted with indicated antibodies. PARP and α-tubulin were used as nuclear and cytoplasmic markers. The signals were measured by ImageJ. The values for the cytoplasmic fraction were set at 1.00. (E, F) SW480 cells were treated with VP-16. Subcellular fractionation was performed. Endogenous RASSF6 was detected with anti-RASSF6 antibody. All of the experiments were repeated three times.

silencing (data not shown). The finding that RASSF6 is accumulated in the nucleus in p53-negative H1299 cells also supports that p53 is not required. BAF60a, a component of SWI/SNF chromatin remodeling complex, has the SWIB domain, which is homologous to the p53-binding domain of MDM2 (22). Therefore, we speculated that RASSF6 may interact with BAF60a. We immunoprecipitated endogenous RASSF6 from SW480 cells and found that endogenous BAF60a was coimmunoprecipitated (Fig. 4A). Importantly, VP-16 treatment enhanced the interaction between RASSF6 and BAF60a (Fig. 4A, arrowhead). VP-16 treatment also augmented the interaction between exogenously expressed

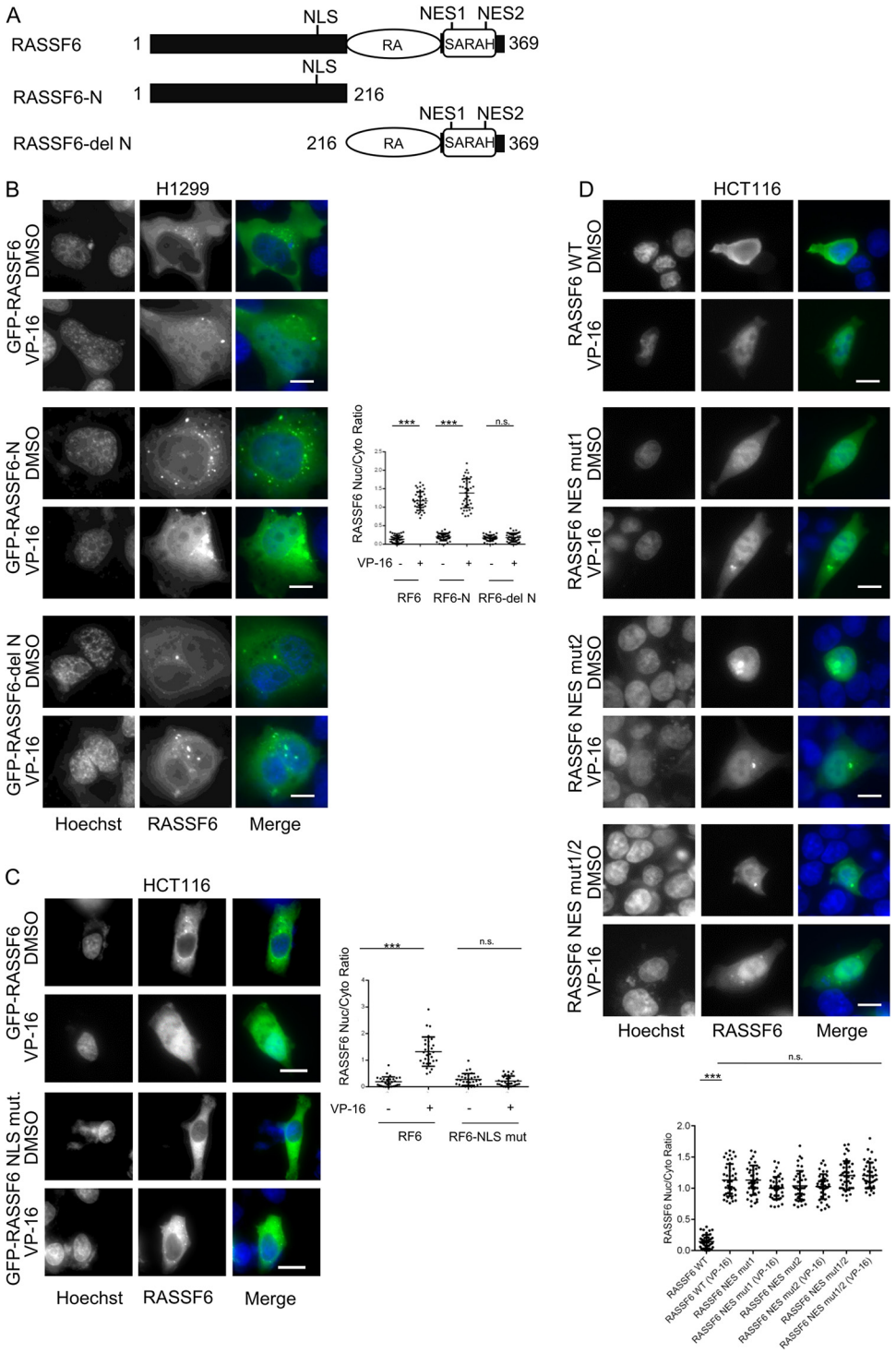

FIG 2 RASSF6 harbors a nuclear localization signal in the N-terminal region. (A) Schematic of RASSF6 constructs. RA, SARAH, NLS, and NES stand for Ras-association domain, Salvador/RASSF/Hippo domain, nuclear localization signal, and nuclear export signal, respectively. Numbers indicate the numbers of amino acid residues. (B, C, D) GFP-RASSF6, RASSSF6-N, and RASSF6-delN were expressed in H1299 cells in panel B. GFP-RASSF6 NLS mutant, RASSF6 NES1 mutant, RASSF6 NES2 mutant, and RASSF6 NES1/2 mutant were expressed in HCT116 cells in panels C and D. The cells were treated, and the distributions of GFP signals were evaluated in the same way as in Fig. 1A. Scale bars, 25 μm. n.s., not significant; ***, $P < 0.001$. The experiments were repeated three times.

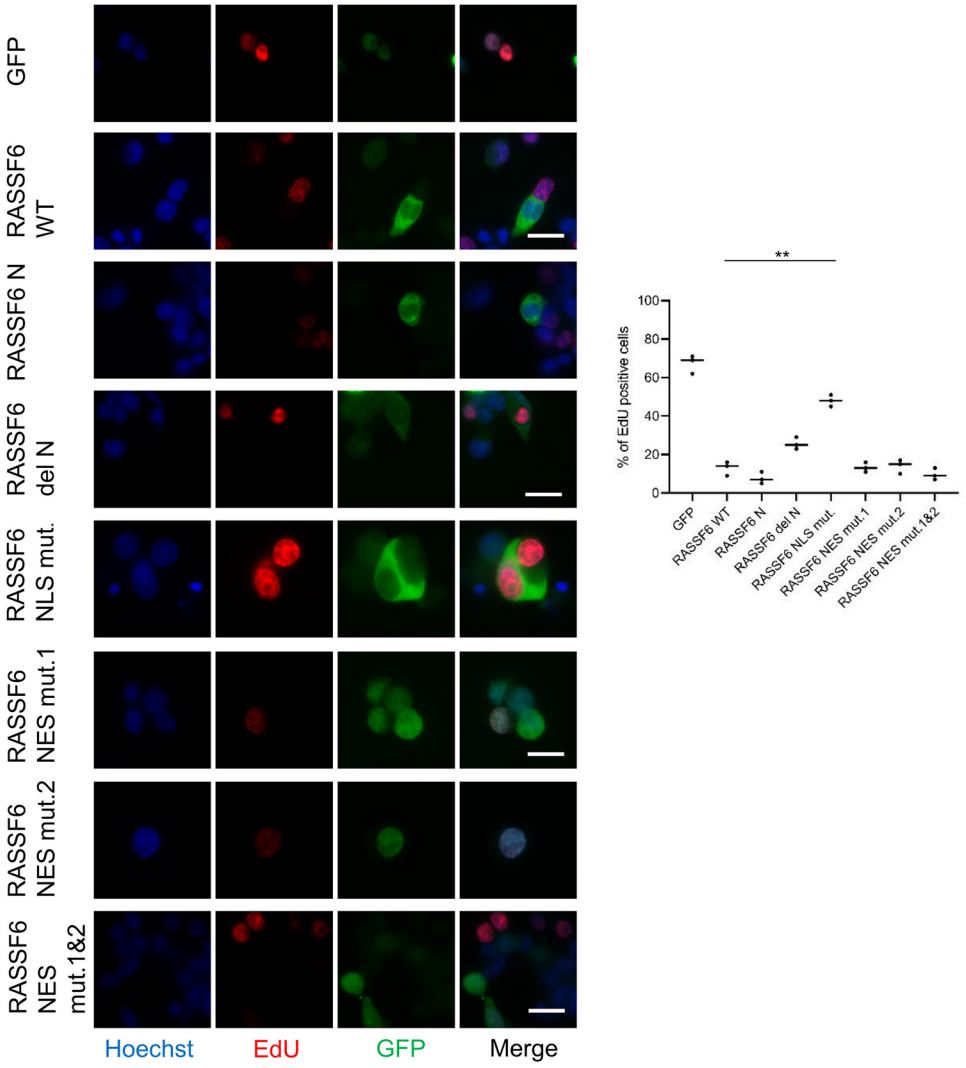

FIG 3 The effect of RASSF6 on EdU incorporation. HCT116 cells were transfected with various pCIneoGFP constructs. EdU incorporation assay was performed as described in Materials and Methods. The nuclei were visualized with Hoechst 33342. Fifty GFP-positive cells were observed for each point. The ratio of the cells incorporating EdU was calculated. Five independent points were taken for each sample. **, $P < 0.01$. Scale bars, 25 μm.

RASSF6 and BAF60a (Fig. 4B, arrowhead). *BAF60a* silencing abolished the DNA damage-induced nuclear accumulation of RASSF6 in HCT116 (Fig. 4C) and H1299 cells (data not shown).

BAF53 is involved in the DNA damage-induced nuclear accumulation of RASSF6. We previously studied a *Caenorhabditis elegans* homologue of RASSF6 (RSF-1) and observed that an *rsf-1* deletion mutant exhibits the actin disorganization (23). The SWI/SNF complex contains BAF53 (also called ACTL6A), which is an actin-like protein (24). Therefore, we further presumed that BAF53 may also bind to RASSF6. Indeed, BAF53 was coimmunoprecipitated with RASSF6 from SW480 cells (Fig. 4D). The interaction was enhanced by VP-16 treatment (Fig. 4D and E, arrowheads). Furthermore, *BAF53* silencing blocked the DNA damage-induced nuclear accumulation of RASSF6 in HCT116 (Fig. 4F) and H1299 cells (data not shown).

RASSF6 strengthens the interaction of BAF60a and BAF53 with p53. We next examined the effect of RASSF6 on the interaction of p53 with BAF53 and BAF60a. At the basal condition, the interaction of p53 with BAF53 or BAF60a was hardly observed (Fig. 5A and B, second lanes), while it became detectable with the coexpression of

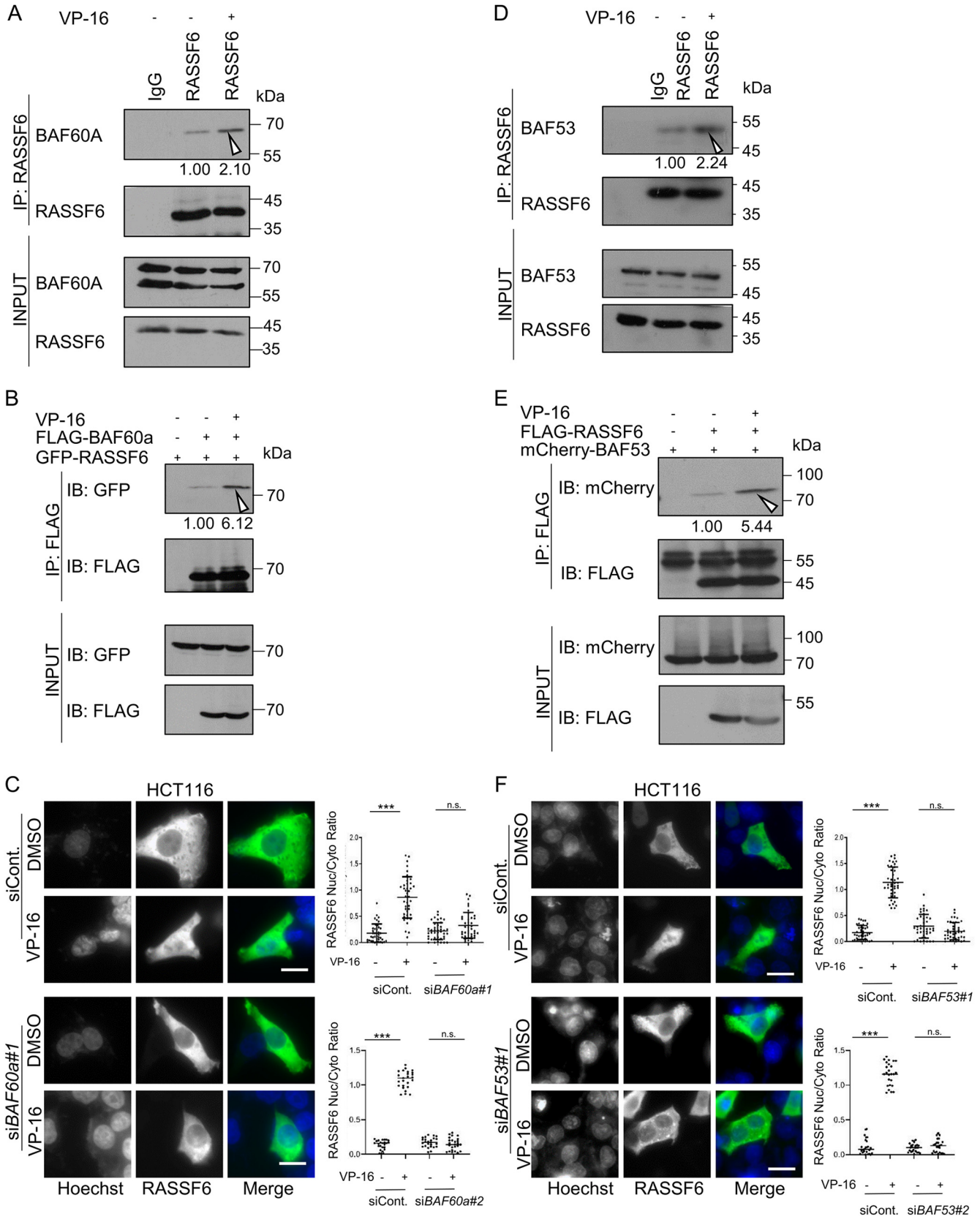

FIG 4 BAF60a and BAF53 interact with RASSF6 and are involved in the nuclear accumulation of RASSF6. (A, D) SW480 cells were treated with either dimethyl sulfoxide (DMSO) or 50 μM VP-16 for 180 min, and RASSF6 was immunoprecipitated. The inputs and immunoprecipitates were immunoblotted with the indicated antibodies. The numbers indicate the relative intensities of signals measured by ImageJ. In two additional experiments, RASSF6 enhanced the signals by

(Continued on next page)

RASSF6 (Fig. 5A and B, third lanes). VP-16 treatment further enhanced the interaction between BAF53 and p53 in the presence of RASSF6 (Fig. 5A, fourth lane), while the additional effect was not remarkable for the interaction between BAF60a and p53 (Fig. 5B, fourth lane). We confirmed these observations in Lumier assay (Fig. 5C and D). Conversely, *RASSF6* silencing attenuated VP-16 treatment-induced enhancement of the binding of p53 to BAF53 or BAF60a (Fig. 5E and F).

RASSF6 directly binds to BAF53, and *BAF53* silencing attenuates the interaction between RASSF6 and BAF60a, while *BAF60a* silencing has no effect on the interaction between RASSF6 and BAF53. We further examined how RASSF6, BAF60a, and BAF53 interact with each other. VP-16 treatment enhanced the interaction between BAF53 and BAF60a (Fig. 6A, arrowheads). *RASSF6* silencing abolished this effect of VP-16 treatment on the interaction between BAF53 and BAF60a (Fig. 6A, si*RASSF6*). The interaction between RASSF6 and BAF53 was still enhanced by VP-16 treatment after *BAF60a* silencing (Fig. 6B). In contrast, VP-16 failed to enhance the interaction between RASSF6 and BAF60a in BAF53-depeleted cells (Fig. 6C, si*BAF53*). Together with the observation that the interaction between RASSF6 and BAF53 is more remarkable than that between RASSF6 and BAF60a, we suspected that DNA damage triggers primarily the interaction between RASSF6 and BAF53. With this speculation, we used purified recombinant proteins and detected the direct interaction between RASSF6 and BAF53 (Fig. 6D).

DNA damage induces CDK9-mediated phosphorylation of BAF53, which enhances the binding of BAF53 to RASSF6. We hypothesized that DNA damage induces the molecular modification of BAF53, which enhances the binding of BAF53 to RASSF6. We examined whether DNA damage would induce the phosphorylation of BAF53 and found that VP-16 treatment triggered the mobility shift of BAF53 in Phos-tag gels (Fig. 7A, arrowhead). A previous study revealed that BAF53 is phosphorylated by CDK9 (25). As expected, LDC000067, CDK9 inhibitor, blocked VP-16 treatment-induced phosphorylation of BAF53 (Fig. 7A, third lane). LDC000067 abolished VP-16 treatment-induced enhancement of the interaction between BAF53 and RASSF6 (Fig. 7B). VP-16 treatment did not enhance the binding of RASSF6 to BAF53 mutant, in which three putative phosphorylation sites (serine 86, serine 195, and serine 233) were mutated to alanine (Fig. 7C). In the pulldown assay, MBP-RASSF6 more efficiently trapped BAF53 from VP-16-treated cells but not from CDK9 inhibitor- and VP-16-treated cells (Fig. 7D). LDC000067 blocked VP-16 treatment-induced nuclear accumulation of RASSF6 in HCT116 and H1299 cells (Fig. 7E and F).

BAF53 and BAF60a are involved in RASSF6-induced TP53 target gene transcription. These findings prompted us to hypothesize that DNA damage induces the nuclear accumulation of RASSF6 and promotes the complex formation of BAF53 and BAF60a in the vicinity of p53 target genes. First, we confirmed the previously reported findings that BAF60a and BAF53 are involved in p53 target gene transcriptions (20, 21). Doxorubicin treatment enhanced the expression of *BAX*, *BTG2*, and *CDKN1A*, while *BAF53* silencing and *BAF60a* silencing partially attenuated the enhancement (Fig. 8A and B). We previously reported that enforced expression of RASSF6 mimics DNA damage-induced p53 target gene transcription (16). Therefore, we examined the effect of *BAF53* silencing and *BAF60a* silencing on RASSF6-induced p53 target gene transcription. Both *BAF53* silencing and *BAF60a* silencing compromised RASSF6-induced p53 target gene transcription in HCT116 cells (Fig. 8C and D).

FIG 4 Legend (Continued)

2.32 and 2.21 for BAF60a and 3.36 and 2.41 for BAF53. (B, E) HEK293FT cells were transfected with pCIneoGFP-RASSF6 and pCIneoFHF-BAF60a in panel B and with pCIneoFHF-RASSF6 and pCIneomCherry-BAF53 in panel E and 24 h later treated with either DMSO or 50 μM VP-16 for 180 min. The immunoprecipitation was performed with anti-DYKDDDDK-tag beads. VP-16 treatment enhances the interaction between RASSF6 and BAF60a (arrowheads). (C, F) HCT116 cells were transfected with control, *BAF60a#1*, *BAF60a#2*, *BAF53#1*, or *BAF53#2* siRNA. Twenty-four hours later, the cells were transfected with pCIneoGFP-RASSF6. Twenty-four hours later, the cells were treated with either DMSO or 50 μM VP-16 for 180 min. The distribution of GFP-RASSF6 was evaluated as in Fig. 1A. Due to the limitation of space, for *BAF60a#2* siRNA and *BAF53#2* siRNA, only the quantified results are shown. n.s., not significant; ***, $P < 0.001$. Scale bars, 25 μm. The experiments were repeated three times.

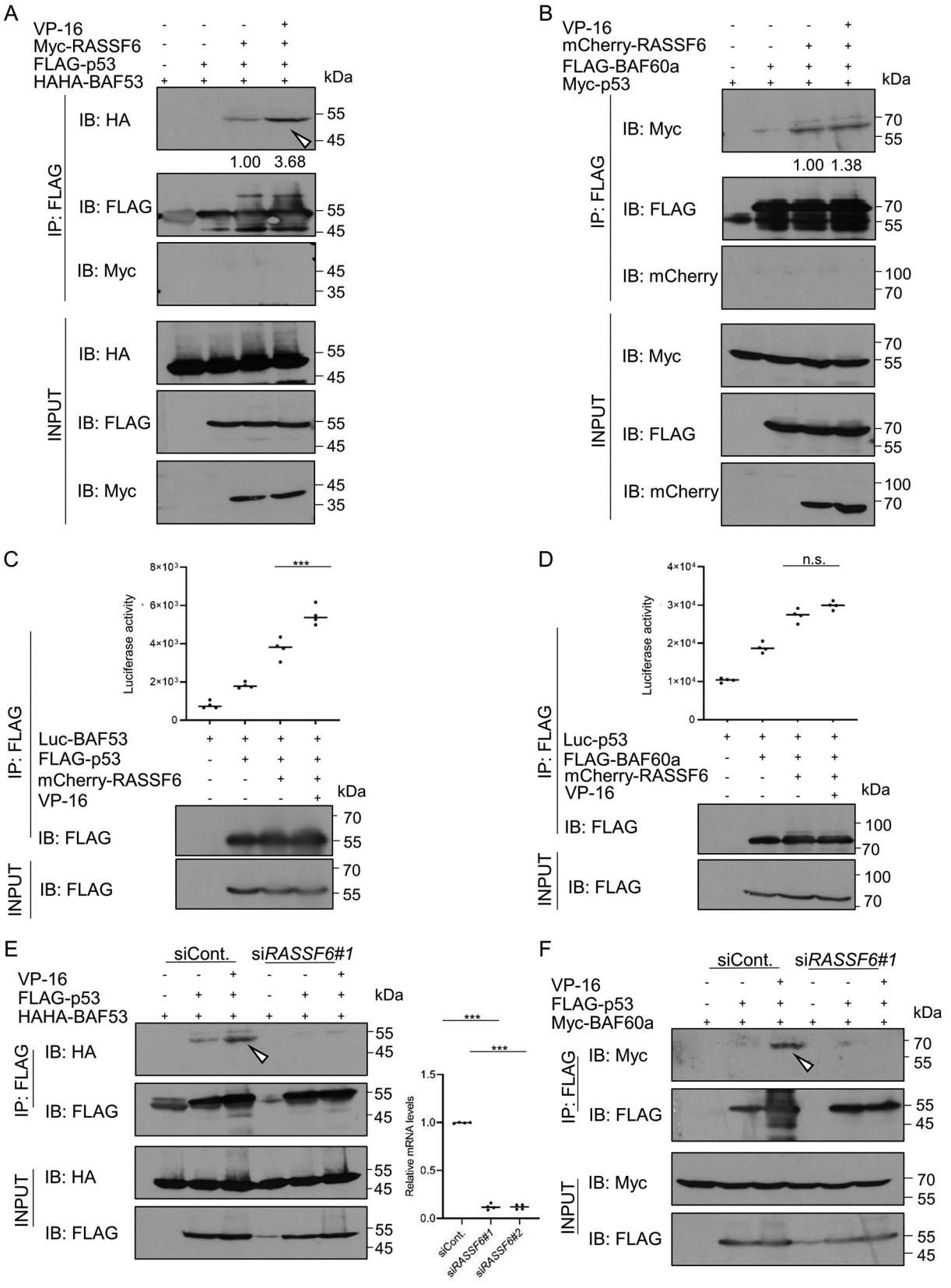

FIG 5 RASSF6 is involved in DNA damage-induced interaction of p53 with BAF53 and BAF60a. (A, B) HEK293FT cells were transfected with pCIneoFHF-p53, pCIneoHAHA-BAF53, and pCIneoMyc-RASSF6 in panel A and pCIneoFHF-BAF60a, pCIneoMyc-p53, and pCIneomCherry-RASSF6 in panel B. Forty-eight hours later, the cells were treated with DMSO or 50 μM VP-16, and the immunoprecipitation was performed

(Continued on next page)

BAF53 and BAF60a are involved in RASSF6-induced apoptosis. Enforced RASSF6 expression induces apoptosis in various cells (1, 2, 14–16). p53 is the most important factor in RASSF6-induced apoptosis. As BAF53 and BAF60a are involved in RASSF6-induced p53 target gene transcription, we next examined the effect of *BAF53* silencing and *BAF60a* silencing on RASSF6-induced apoptosis. *BAF53* silencing reduced RASSF6-induced cytochrome *c* release, apoptosis-inducing factor (AIF) release, and nuclear condensation in HCT116 cells (Fig. 9). *BAF60a* silencing also showed a similar effect (Fig. 10). We also evaluated RASSF6-induced apoptosis by detecting caspase-3 cleavage and confirmed the effect of *BAF53* silencing and *BAF60a*-silencing (Fig. 11).

DISCUSSION

There are 10 *RASSF* genes in the human genome (26–29). Among them, *RASSF1* to *RASSF6* encode proteins with a RAS-association domain and a SARAH/RASSF/Hippo (SARAH) domain. All of these genes are silenced in human cancers, and their low expression is associated with poor clinical outcome. Thus, these genes are regarded as tumor suppressor genes, although *RASSF1C*, a variant of RASSF1, is oncogenic (30, 31).

We originally identified RASSF6 as a protein interacting with PDZ domain-containing membrane-associated proteins (2). Thereafter, we revealed that RASSF6 interacts with various molecules, including mammalian Ste20-like kinases, RAS proteins, MDM2, BCL-XL, pRb, BMI1, and UNC119 (14, 16, 19, 32, 33). These studies prompted us to question whether RASSF6 interacts with each partner in the cytoplasm or in the nucleus. For instance, as UNC119 is a cytoplasmic protein, the interaction between RASSF6 and UNC119 should occur in the cytoplasm. However, pRb recruits RASSF6 into the nucleus (19). As pRb is a nuclear protein, RASSF6 must be in the nucleus to be trapped by pRb. Oncogenic KRAS recruits MDM2 via RASSF6 from the nucleus to the cytoplasm in H1299 cells, which suggests that RASSF6 once enters the nucleus, binds MDM2, and then exits the nucleus together with MDM2 (18). These findings imply that RASSF6 shuttles between the cytoplasm and the nucleus and that the subcellular distribution is regulated in the cellular context-dependent manner.

RASSF6 has a typical NLS signal in the N-terminal region. RASSF6 mutant, in which this signal is mutated, is distributed exclusively in the cytoplasm. Hence, we can conclude that this NLS is essential for RASSF6 to enter the nucleus. In contrast, the molecular determinant of the nuclear export is ambiguous. There are two NES candidates, and when one of them is mutated, RASSF6 is accumulated in the nucleus, which suggests that both of them are necessary for RASSF6 to be exported from the nucleus. However, as these two sites reside in the SARAH domain, we could not exclude the possibility that the mutations nonspecifically disturb the structure of this coiled-coil region and disturb the subcellular distribution of RASSF6.

Importantly, DNA damage triggers the nuclear accumulation of RASSF6. We found that DNA damage induces CDK9-mediated phosphorylation of BAF53 and that CDK9

FIG 5 Legend (Continued)
with anti-DYKDDDDK-tag beads. VP-16 augmented the binding of BAF53 to p53 in the presence of RASSF6 (arrowhead). The numbers indicate the relative intensities of signals measured by ImageJ. In two additional experiments, VP-16 enhanced the signals by 3.16 and 2.01 for BAF53 and p53 and 1.48 and 1.60 for BAF60a and p53 under the coexpression of RASSF6. (C, D) HEK293FT cells were transfected with pCIneoLuc-BAF53 and pCIneoFHF-p53 in panel C and pCIneoLuc-p53 and pCIneoFHF-BAF60a in panel D without or with pCIneomCherry-RASSF6 and 24 h later treated with either DMSO or 50 μM VP-16 for 180 min. The immunoprecipitation was performed with anti-DYKDDDDK-tag beads. Luciferase activity in the immunoprecipitates were measured by PicaGene as a substrate. n.s., not significant; ***, $P < 0.001$. (E, F) HEK293FT cells were transfected with control siRNA, *RASSF6#1* siRNA, or *RASSF6#2* siRNA. Twenty-four hours later, the cells were transfected with pCIneoHAHA-BAF53 and pCIneoFHF-p53 in panel E and pCIneoFHF-p53 and pCIneoMYC-BAF60a in panel F. Twenty-four hours later, the cells were treated with either DMSO or 50 μM VP-16 for 180 min. The immunoprecipitation was performed with anti-DYKDDDDK-tag beads. The experiments were repeated three times. The validation of *RASSF6* silencing was performed by quantitative reverse transcriptase PCR (qRT-PCR). We confirmed the similar results using two *RASSF6* siRNAs. Due to the space limitation, the results for *RASSF6#2* siRNA are not shown. Arrowheads indicate the enhanced interaction of p53 with BAF53 or BAF60a, which is not detected after *RASSF6* silencing. ***, $P < 0.001$.

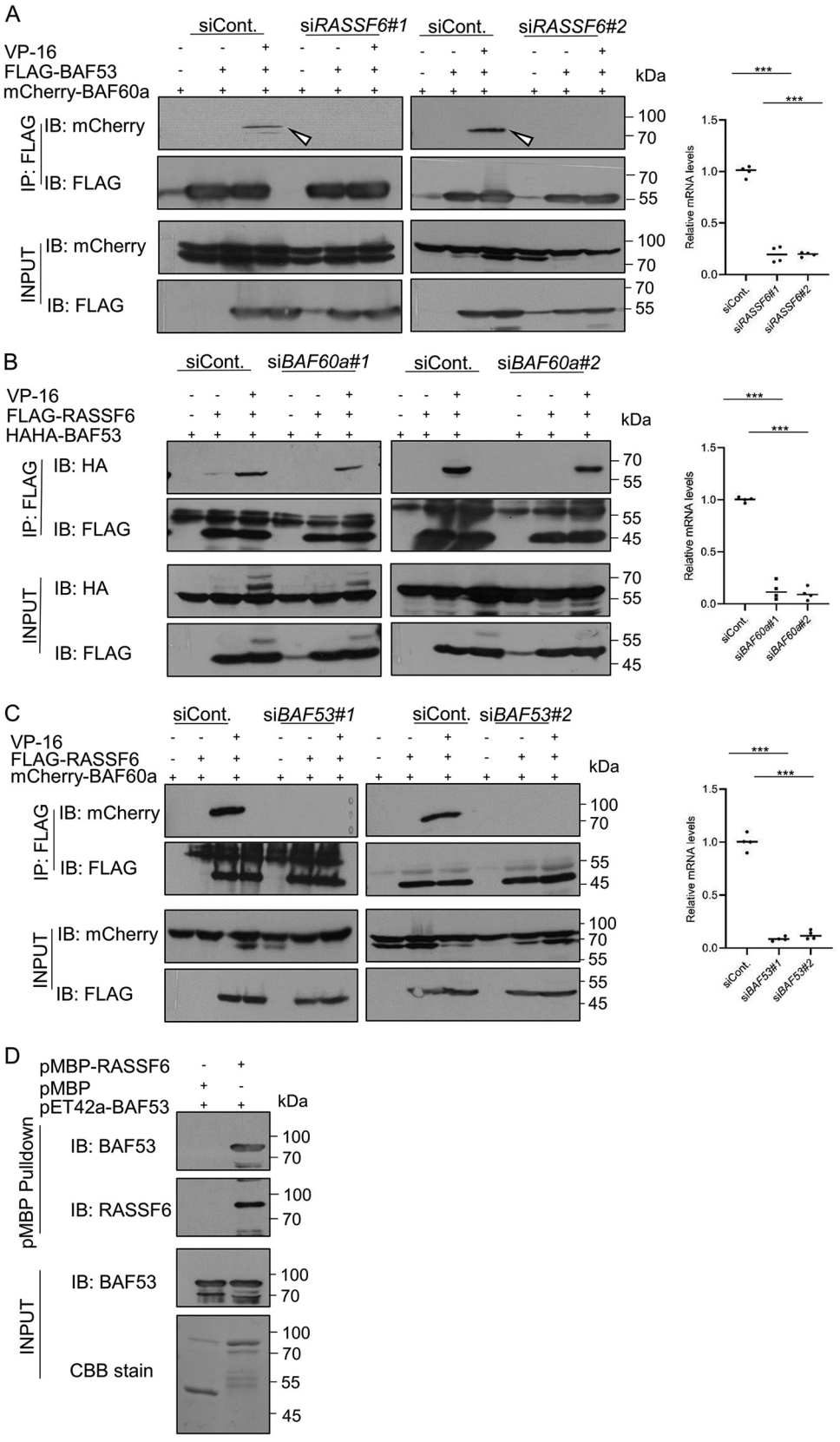

FIG 6 RASSF6 is involved in DNA damage-induced interaction between BAF53 and BAF60a and directly binds to BAF53. HEK293FT cells were transfected with control siRNA, *RASSF6* siRNAs, *BAF60a* siRNAs, and *BAF53* siRNAs as indicated. Twenty-four hours later, the cells were transfected with pCIneoFHF-BAF53 and pCIneomCherry-BAF60a in

(Continued on next page)

inhibitor blocks the nuclear accumulation of RASSF6. Therefore, we propose the model that DNA damage activates CDK9 to phosphorylate BAF53 and that phosphorylated BAF53 traps RASSF6 in the nucleus and subsequently promotes the formation of BAF53-BAF60a-p53 complex. Thus, in the presence of RASSF6, BAF53, and BAF60a, the components of SWI/SNF chromatin remodeling complex more tightly bind to p53 and activate p53 target gene transcription (Fig. 12). CDK9 is identified as a component of the replication stress response (34). CDK9 interacts with ATR kinase and checkpoint signaling proteins. Therefore, it is comprehensible that CDK9 is activated in response to DNA damage caused by VP-16 treatment and UV exposure. However, in our study, the ATR kinase inhibitor did not block the nuclear accumulation of RASSF6, which implies that CDK9 is activated independent of ATR. Further studies will be necessary to elucidate such an unidentified regulatory pathway. Moreover, as we previously reported, RASSF6 forms a complex with mammalian Ste20-like (MST) kinases in basal condition and MST blocks RASSF6-induced apoptosis (14). As MST kinases are mainly localized in the cytoplasm, it is reasoned that MST kinases block the nuclear accumulation of RASSF6. It will be interesting to examine whether and how MST kinases affect the interaction between RASSF6 and BAF53 in basal condition and after DNA damage.

MATERIALS AND METHODS

DNA construction. pCIneoGFP-RASSF6, pCIneoFHF-RASSF6, pCIneoGFP-RASSF6-N, pCIneoRASSF6-delN, pCIneoMy-p53, pCIneoFHF-p53, pCIneoLuc, pCIneomCherry, and pMal-RASSF6 were described previously (16–18). The pCIneoGFP-RASSF6 NLS mutant, NES1 mutant, NES2 mutant, and NES1/2 mutant were generated by using the primers listed in Table S1 in the supplemental material. Human BAF53 and BAF60a cDNAs were obtained by PCR using the primers listed in Table S1 and human kidney and lung cDNA libraries. PCR products were digested with MluI and SalI and ligated into pCIneoFHF, pCIneomCherry, pCIneoHAHA, and pCIneoLuc to generate pCIneoFHF-BAF53, pCIneoHAHA-BAF53, pCIneomCherry-BAF53, pCIneoFHF-BAF60a, pCIneomCherry-BAF60a, and pCIneoLuc-BAF53. The EcoRI/SalI fragment from pCIneoFHF-p53 was ligated into the same sites of pCIneoLuc to generate pCIneoLuc-p53. The primers used for the construction of pET42a-BAF53 were also listed in Table S1. BAF53 mutants were generated by PCR using the primers listed in Table S1.

Antibodies and reagents. The antibodies and the reagents were obtained from commercial sources as follows: rabbit anti-GFP (598), rabbit α-tubulin (PM054), and rabbit Myc (562) (Medical and Biological Laboratories Co. Ltd., Nagoya, Japan); rat anti-HA (3F10), pepstatin A (P5318), Y27632 (Y0503), and Hoechst 33342 (Sigma-Aldrich, Dallas, TX, USA); anti-DYKDDDDK-tag (014-22383), anti-DYKDDDDK-tag beads (016-22784), latrunculin A (125-04363), and leupeptin (334-40414) (Wako Pure Chemical Industries, Osaka, Japan); MG-132 (Nacalai Tesque, Tokyo, Japan); rabbit anti-RASSF6 (11921-1-AP) (Proteintech, Rosemond, USA); protein G-Sepharose 4 fast flow (GE Healthcare, Little Chalfont, United Kingdom); mouse anti-cytochrome *c* (6H2 B4) (556432) (BD Biosciences, San Jose, CA, USA); mouse anti-Myc (9E10) (American Type Culture Collection, Manassas, VA, USA); mouse PARP (sc-74470), etoposide (VP-16) (sc-3512), mouse BAF60a (sc-135843), mouse BAF53 (sc-137062), and mouse AIF (sc-13116) (Santa Cruz Biotechnology, Dallas, TX, USA); mouse Alexa 488 (A11029) (Life Technologies, Carlsbad, CA, USA); rabbit mCherry (GTX59788) (GeneTex, Irvine, CA, USA); rabbit anti-cleaved caspase 3 (Asp175) (9661) (Cell Signaling Technology); KU-55933 (16336), AZ20 (17589), NU7441 (14881), cytochalasin D (11330), Saracatinib (11497), SP 600125 (10010466), and LDC000067 (29419) (Cayman Chemical, Ann Arbor, MI, USA); and BAPTA-AM (B035) (Dojindo, Kumamoto, Japan).

Cell cultures, transfection, and infection. HEK293FT, HCT116, SW480, and H1299 cells were cultured in Dulbecco's modified Eagle medium containing 10% (vol/vol) fetal bovine serum and 10 mM HEPES-NaOH (pH 7.4) under 5% CO_2 at 37°C. Transfection was performed with Lipofectamine 2000 (Thermo Fisher Scientific, Waltham, MA, USA).

Immunoprecipitation of RASSF6 from SW480 cells. SW480 cells, which were plated at 50 to 60% confluence in one 100-mm dish, were suspended in 1 mL of the lysis buffer (25 mM Tris-HCl [pH 7.4], 100 mM NaCl, 1 mM EDTA, 1 mM EGTA, 0.5% [wt/vol] sodium deoxycholate, 1% [vol/vol] TritonX-100, 10% glycerol, 50 μM 4-Amidinophenylmethanesulfonyl fluoride [APMSF], 3 mg/L pepstatin A,

FIG 6 Legend (Continued)
panel A, pCIneoFHF-RASSF6 and pCIneoHAHA-BAF53 in panel B, and pCIneoFHF-RASSF6 and pCIneomCherry-BAF60a in panel C. Twenty-four hours later, the cells were treated with either DMSO or 50 μM VP-16 for 180 min. The immunoprecipitation was performed with anti-DYKDDDDK-tag beads. The experiments were repeated three times. The validation of *RASSF6* silencing, *BAF60a* silencing, and *BAF53* silencing was performed by qRT-PCR. The experiments were repeated three times. (D) Purified His-tagged BAF53 was incubated with either control maltose-binding protein (MBP) or MBP-fused RASSF6 fixed on amylose beads *in vitro*. After washing, the beads were stained with Coomassie blue or immunoblotted with anti-BAF53 antibody.

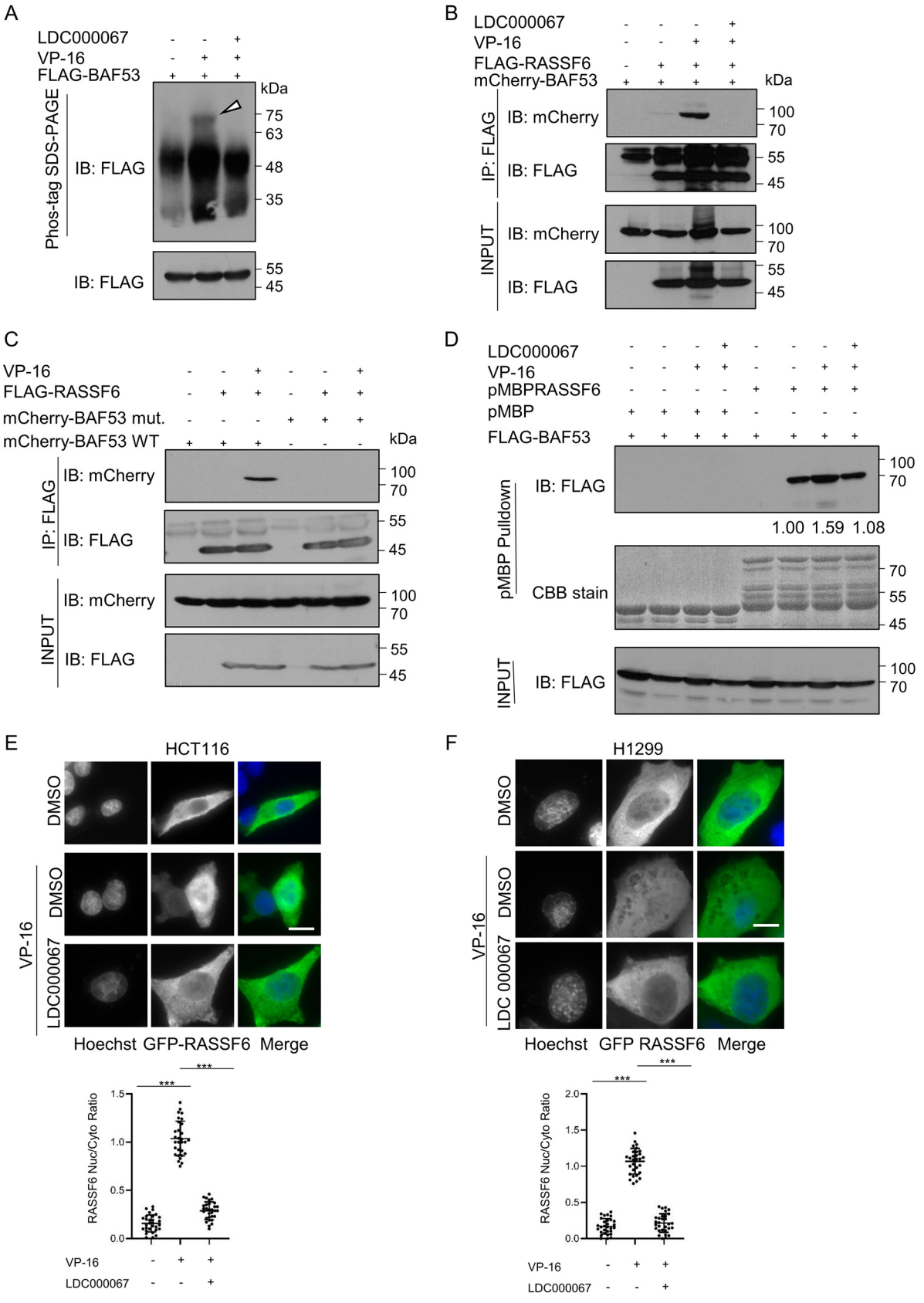

FIG 7 VP-16 treatment triggers CDK9-mediated BAF53 phosphorylation and CDK9 inhibitor blocks the nuclear accumulation of RASSF6. (A) HCT116 cells were transfected with pCIneoFHF-BAF53. Twenty-four hours later, the cells were treated with either DMSO or 50 μM VP-16 in

(Continued on next page)

10 mg/L leupeptin, and 10 μM MG-132), and centrifuged at 20,000 $\times$ *g* for 10 min. The supernatant was incubated with 1 μg of rabbit anti-RASSF6 antibody or control rabbit IgG overnight at 4°C and was incubated with protein G-Sepharose 4 fast-flow beads (GE Healthcare, Chicago, IL, USA) for 2 h at 4°C. The beads were washed four times with the lysis buffer.

Coimmunoprecipitation for exogenously expressed proteins. HEK293FT cells were plated at 1 $\times$ 10^5 cells/well in a 6-well plate. Twenty-four hours later, transfection was performed with Lipofectamine 2000. Twenty-four hours later, the cells were harvested and lysed in 500 μL of the lysis buffer (25 mM Tris-HCl [pH 7.4], 100 mM NaCl, 1 mM EDTA, 1 mM EGTA, 0.5% [wt/vol] sodium deoxycholate, 1% [vol/vol] TritonX-100, 10% glycerol, 50 μM APMSF, 3 mg/L pepstatin A, 10 mg/L leupeptin, and 10 μM MG-132), and centrifuged at 20,000 $\times$ *g* for 10 min. The supernatant (the input) was incubated with 5 μL of anti-DYKDDDDK-tag beads. The beads were washed with the lysis buffer. The proteins in the inputs and the immunoprecipitates were detected with appropriate antibodies.

***In vitro* pulldown assay.** Control MBP and MBP-RASSF6 were expressed in Rosetta DE3 pLysS (Merck) and purified by amylose resin (New England BioLabs, Ipswich, MA, USA). pET42a-BAF53 was also expressed in Rosetta DE3 pLysS. *Escherichia coli* was lysed in 50 mM Tris-HCl [pH 8.0], 0.3 M NaCl, and 6 M urea by sonication. The lysates were centrifuged at 16,000 $\times$ *g* for 10 min to collect the supernatant, which was incubated with NiNTA beads (Qiagen, Hilden, Germany). After the beads were washed with 10 mM Tris-HCl (pH 8.0), 40 mM imidazole, and 0.5% (vol/vol) Triton X-100, His-tagged BAF53 was eluted with 10 mM Tris-HCl (pH 8.0) and 250 mM imidazole. A total of 120 pmol of His-tagged BAF53 was incubated with control MBP or MBP-RASSF6-fixed amylose resin in the buffer (10 mM Tris-HCl [pH 8.0], 2 mM $MgCl_2$, 50 mM APMSF, 3 mg/L pepstatin, and 10 mg/L leupeptin) for 2 h. The resin was washed with the same buffer four times, and the precipitates were stained with Coomassie brilliant blue and immunoblotted with anti-BAF53 or anti-RASSF6 antibody.

Lumier assay. Luciferase-fused proteins were coexpressed with FLAG-tagged proteins in HEK293FT cells. Immunoprecipitation was performed with anti-DYKDDDDK-tag beads. The luciferase activity in the immunoprecipitates was assayed using PicaGene (Toyo Ink) as a substrate.

EdU incorporation assay. HCT116 cells were plated at plated at 5 $\times$ 10^4 cells/well in a 12-well plate. Twenty-four hours later, the cells were transfected with control pCIneoGFP or various pCIneoGFP-RASSF6 vectors. Six hours after transfection, the cells were treated with 2 mM thymidine, cultured for 18 h, and then released from the thymidine block. Two hours later, the cells were treated with 10 μM EdU for 1 h, fixed, and immunostained with anti-EdU antibody.

Immunofluorescence. HCT116 cells were fixed with 3.7% (wt/vol) formaldehyde in phosphate-buffered saline (PBS) at room temperature for 15 min and quenched with 50 mM glycine/PBS. After incubating with 0.2% (vol/vol) Triton X-100 in PBS for another 15 min, the samples were permeabilized with PBS containing 1% (wt/vol) bovine serum albumin (BSA) and 0.1% (vol/vol) Triton X-100 and then incubated with various primary and secondary antibodies. Nuclei were visualized with Hoechst 33342 (Sigma-Aldrich). The images were obtained with a Leica TCS SP8 (Leica Biosystems, Wetzlar, Germany).

The analysis of RASSF6 distribution. GFP fluorescence intensity in H1299 and HCT116 cells expressing GFP-RASSF6 was measured with ArrayScan VTI (Cellomics) using an algorithm for data acquisition designed by vHCS Scan software. Briefly, each cell stained with Hoechst 33342 was identified within the field. The area 2 pixels inside the nuclear boundary was defined as the nuclear area to minimize the cytoplasmic contamination. The ring with the width of 5 pixels around the nuclear boundary was defined as the cytoplasmic area. GFP fluorescence intensity was averaged over the measured area. The ratio of the nuclear GFP over the cytoplasmic GFP was calculated by using BioApplication Compartment Analysis V4 (Thermo Fisher Scientific) in 30 to 150 cells for each sample. The images were obtained with a Leica TCS SP8 (Leica Biosystems, Wetzlar, Germany).

Subcellular fractionation. Cells, which were plated at 70 to 80% confluence in 60-mm dishes, were washed with ice-cold PBS, harvested in PBS by scraping, collected by centrifugation at 4°C, and resuspended with 200 μl of the hypotonic buffer (10 mM HEPES-NaOH [pH 7.5], 10 mM KCl, 1.5 mM $MgCl_2$, 0.34 M sucrose, 10% [vol/vol] glycerol, 0.05% [vol/vol] Nonidet P-40, 50 mM APMSF, 10 mg/L leupeptin, 3 mg/L pepstatin, 50 mM NaF, 2 mM Na_3VO_4, and 25 mM β-glycerophosphate). After being kept at 4°C for 5 min, cells were gently resuspended by pipetting. A total of 66.6 μl of the mixture was saved as the whole cell lysate. The remaining samples were centrifuged at 800 $\times$ *g* at 4°C for 5 min. The supernatant was centrifuged at 20,000 $\times$ *g* for 10 min at 4°C. Ninety microliters of the supernatant was saved as the cytosolic fraction. The pellet was washed twice with the hypotonic buffer, suspended with 133.3 μl of the hypotonic buffer, and saved as the nuclear fraction.

FIG 7 Legend (Continued)
the presence of 50 μM LDC000067 for 180 min. The cell lysates were run on Phos-tag gels and immunoblotted with anti-FLAG antibody. VP-16 induced the shift of BAF53 (arrowhead). (B) HEK293FT cells were transfected with pCIneomCherry-BAF53 and pCIneoFHF-RASSF6. Twenty-four hours later, the cells were treated with either DMSO or 50 μM VP-16 in the presence of 50 μM LDC000067 for 180 min. The immunoprecipitation was performed with anti-DYKDDDDK-tag beads. The experiments were repeated three times. (C) The same experiment as in panel B was performed using the pCIneomCherry-BAF53 mutant, in which three CDK9-phosphorylation sites are mutated to alanine. (D) HEK293 cells were transfected with pCIneFHF-BAF53 and treated with DMSO, VP-16, or VP-16/LDC000067. The cell lysates were incubated with either control MBP or MBP-RASSF6 fixed on amylose resin. FLAG-tagged BAF53a attached to the beads was detected with anti-DYKDDDDK antibody. The intensities of the signals were measured by ImageJ. The value of the signal for the basal condition was set at 1.0. (E, F) HCT116 and H1299 cells expressing GFP-RASSF6 were pretreated with 50 μM LDC000067 for 30 min and then exposed to 50 μM VP-16 for 180 min. The distribution of GFP-RASSF6 was evaluated as in Fig. 1A. ***, $P < 0.001$. Scale bars, 25 μm.

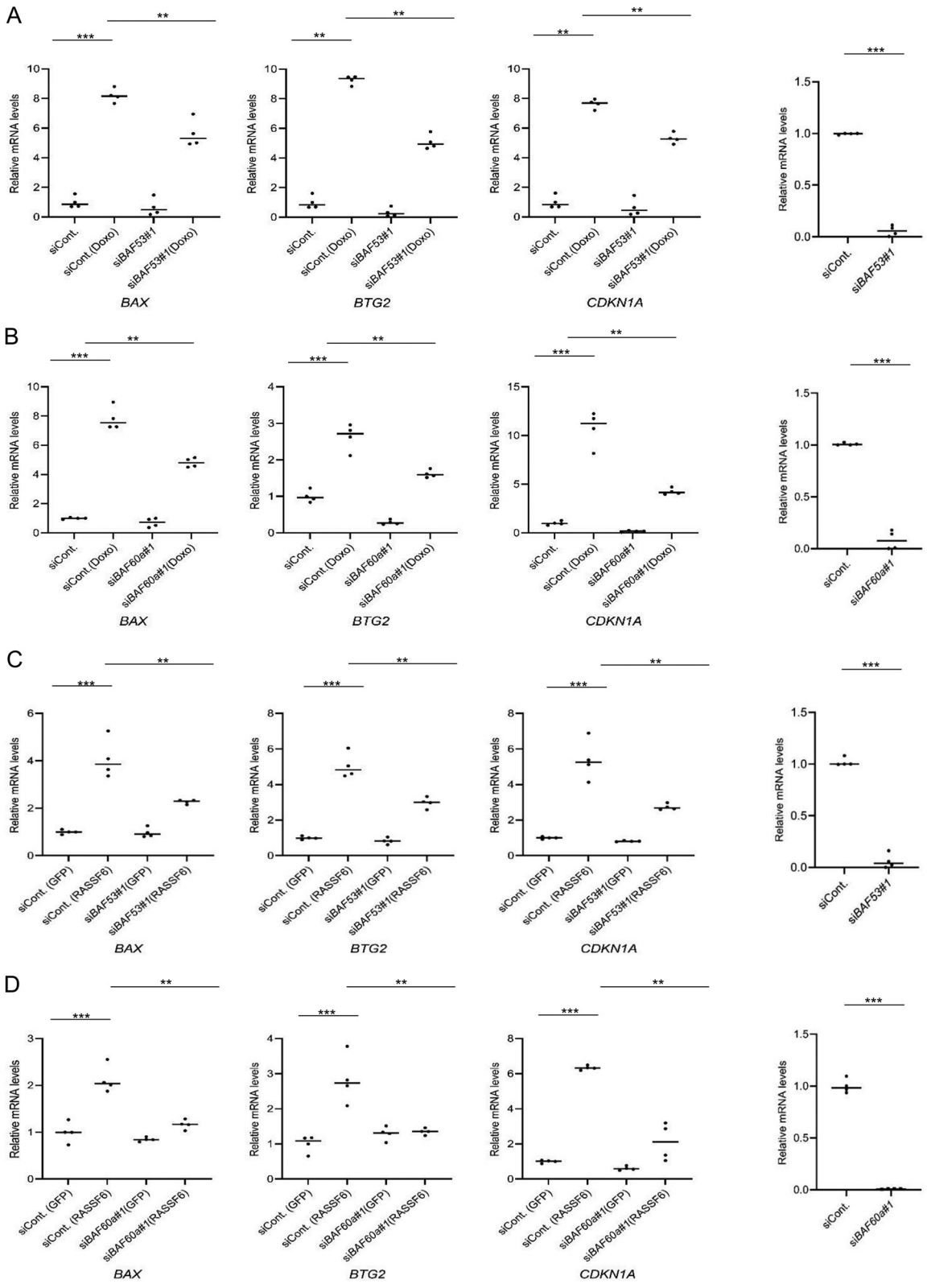

FIG 8 BAF53 and BAF60a are involved in doxorubicin-induced and RASSF6-mediated p53 target gene transcription. (A, B) HCT116 cells were transfected with control siRNA, *BAF53#1* siRNA, or *BAF60a#1* siRNA. Twenty-four hours later, the cells were treated with either DMSO or 50 μM doxorubicin for 180 min. Twenty-four hours later, mRNAs were collected, and qRT-PCR was performed. (C, D) HCT116 cells were transfected with control siRNA, *BAF53#1* siRNA, or *BAF60a#1* siRNA. Twenty-four hours later, the cells were transfected with control pCIneoGFP or pCIneoGFP-RASSF6. Twenty-four hours later, mRNAs were collected, and qRT-PCR was performed in quadruplicates for each sample. The validation of *BAF53* silencing and *BAF60a* silencing was performed by qRT-PCR. The experiments were repeated three times. **, $P < 0.01$; ***, $P < 0.001$.

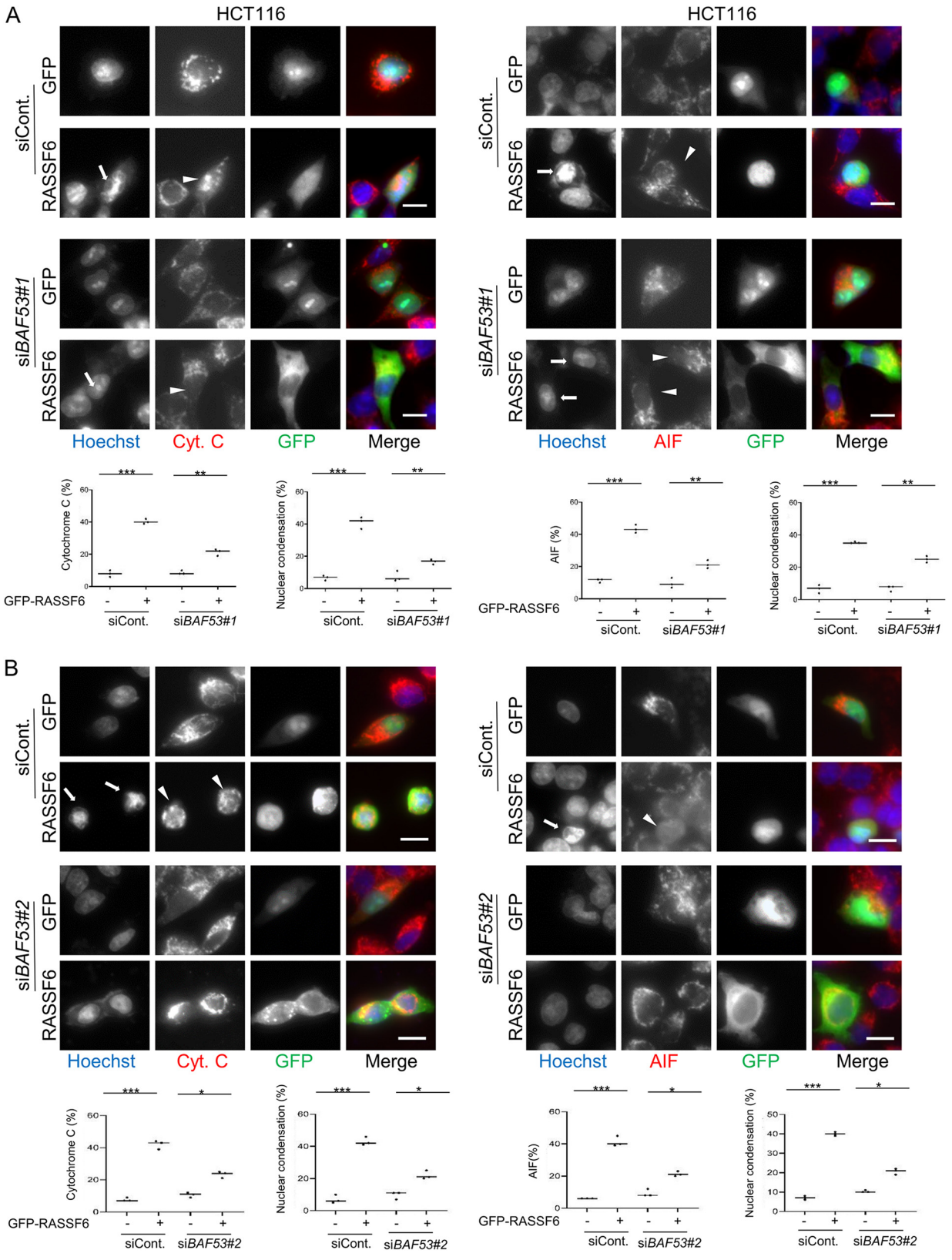

FIG 9 BAF53 is involved in RASSF6-induced cytochrome *c* release, AIF release, and nuclear condensation. HCT116 cells were transfected with control siRNA, *BAF53#1* siRNA in panel A, and *BAF53#2* siRNA in panel B. Twenty-four hours later, the cells were transfected with control pCIneoGFP or pCIneoGFP-RASSF6. Twenty-four hours later, the cells were immunostained with anti-cytochrome *c* or anti-AIF antibody. Nuclei were visualized with Hoechst 33342. The ratios of cells exhibiting cytochrome *c* release, AIF release, and nuclear condensation were evaluated in 50 GFP-positive cells in each point, and three points were taken for each sample. Scale bars, 25 μm. *, $P < 0.05$; **, $P < 0.01$; ***, $P < 0.001$.

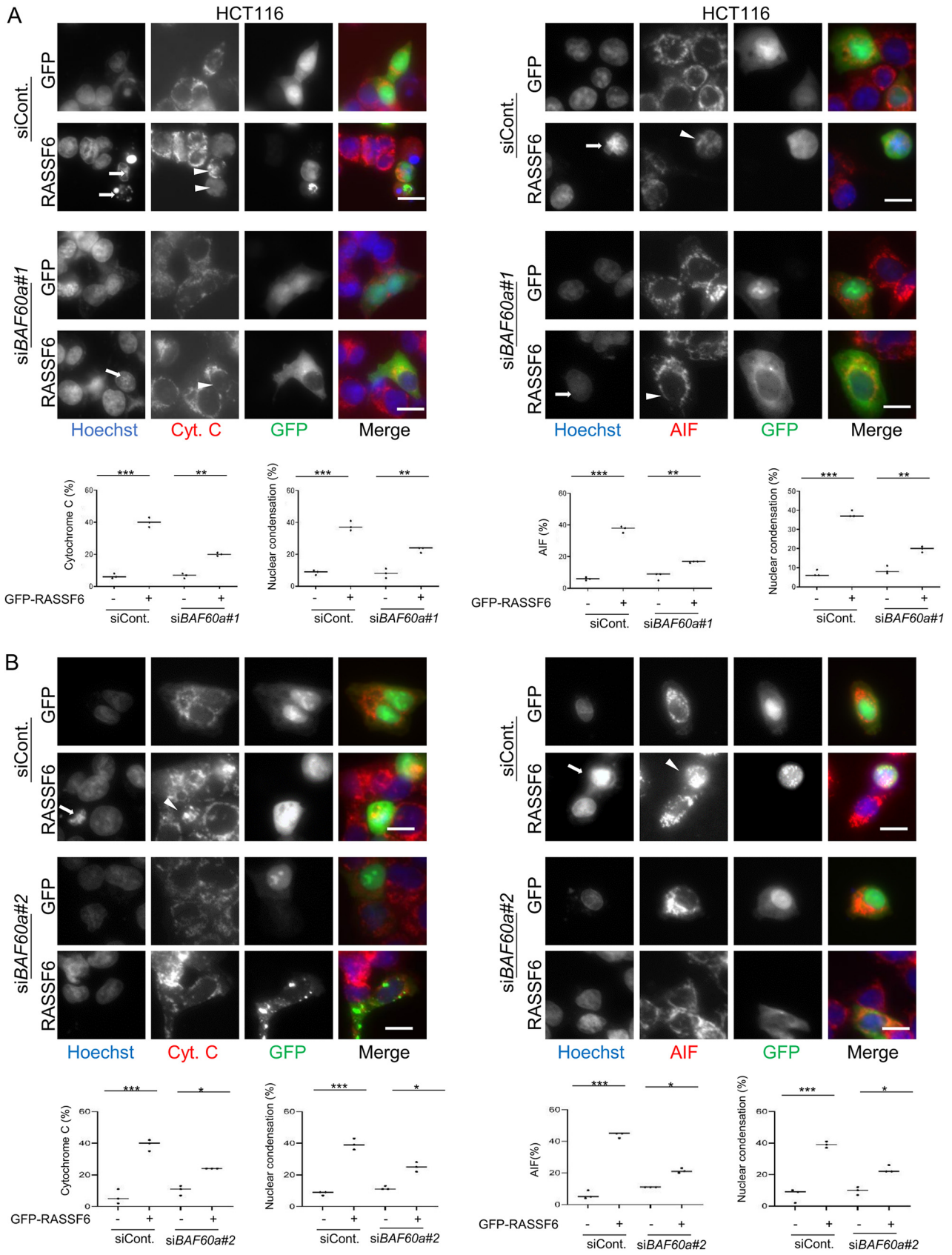

FIG 10 BAF60a is involved in RASSF6-induced cytochrome *c* release, AIF release, and nuclear condensation. HCT116 cells were transfected with control siRNA, *BAF60a#1* siRNA in panel A, and *BAF60a#2* siRNA in panel B. The same experiments as described in Fig. 9 were performed. Scale bars, 25 μm. *, $P < 0.05$; **, $P < 0.01$; ***, $P < 0.001$.

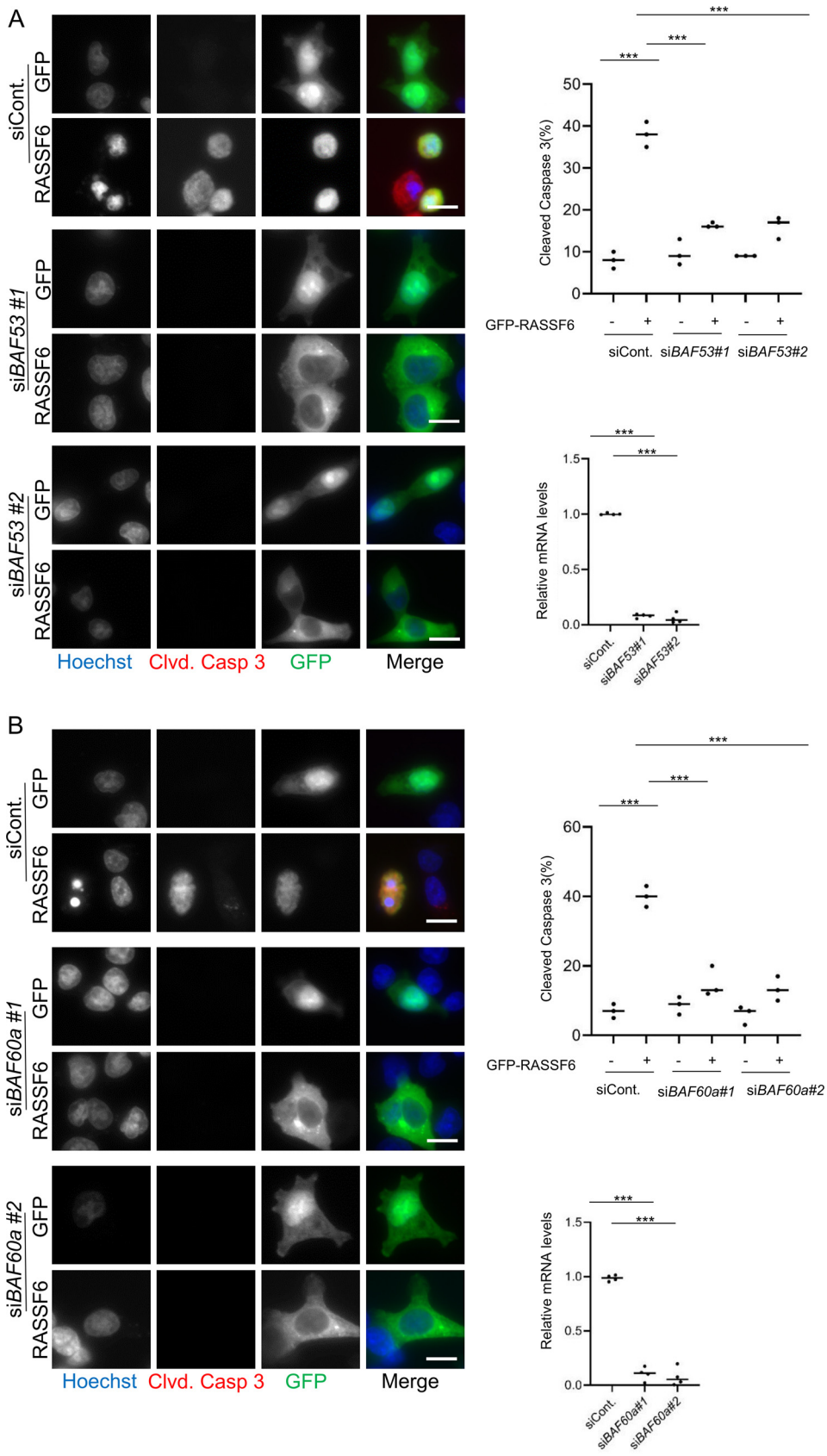

FIG 11 BAF53 and BAF60a are involved in RASSF6-induced caspase-3 cleavage. The same experiments as described in Fig. 9 and 10 were performed. Apoptosis was evaluated with caspase 3 cleavage. The validation of *BAF53* silencing and *BAF60a* silencing was performed by qRT-PCR. Scale bars, 25 μm. *, $P < 0.05$; **, $P < 0.01$; ***, $P < 0.001$.

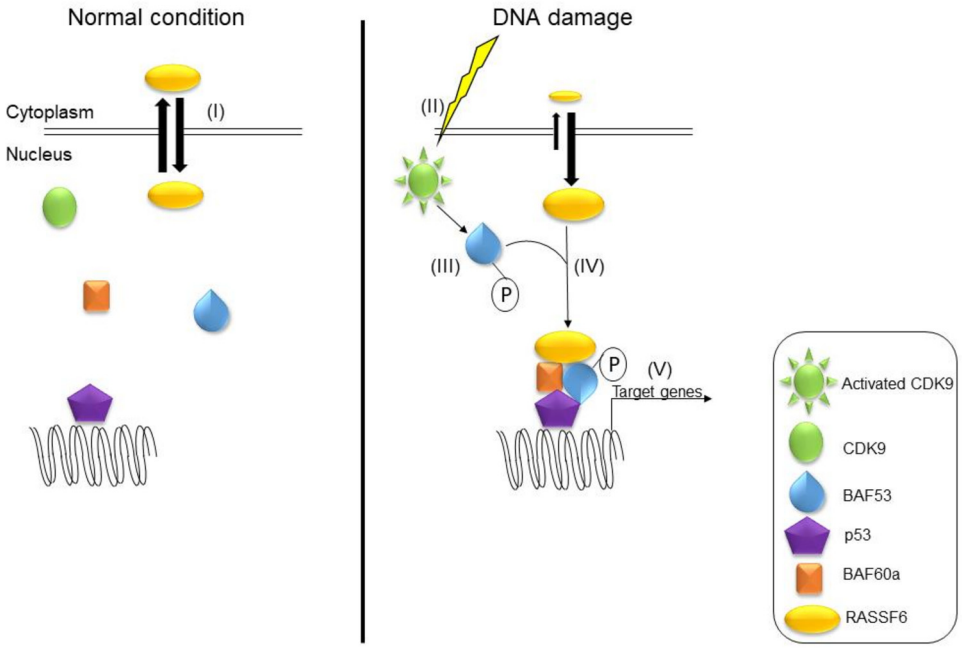

FIG 12 The putative molecular mechanism, by which RASSF6 promotes the formation of BAF53-BAF60a-p53 complex in response to DNA damage and activates p53 target gene transcription. RASSF6 shuttles between the cytoplasm and the nucleus (I). DNA damage activates CDK9 (II), which phosphorylates BAF53 (III). Phosphorylated BAF53 traps RASSF6 in the nucleus (IV). RASSF6 promotes the formation of the BAF53-BAF60a-p53 complex (V).

Evaluation of apoptosis. HCT116 cells were transfected with control pCIneoGFP or pCIneoGFP-RASSF6. Twenty-four hours later, the cells were immunostained with anti-cytochrome *c* or anti-AIF antibody and then nuclei visualized with Hoechst 33342. Cytochrome *c* release, AIF release, cleavage of caspase-3, or the nuclear condensation was evaluated in 50 GFP-positive cells.

RNA interference. Small interfering RNAs (siRNAs) were transfected by Lipofectamine RNAiMAX (Thermo Fisher Scientific). siRNAs were as follows: Silencer Select negative control no. 2 (4390846), human *RASSF6#1* (s46640), human *RASSF6*#2 (s46639), human *MDM2* (s8629), human *TP53* (s605), human *BAF53*#2 (s962), and human *BAF60a#2* (s13151) (Thermo Fisher Scientific); and human *BAF53#1* (sc-60239) and human *BAF60a#1* (sc-72597) (Santa Cruz Biotechnology).

Quantitative RT-PCR. SYBR green (Roche) and ABI7500 real-time PCR system (Applied Biosystem) were used for Quantitative reverse transcriptase PCR (RT-PCR) using the primers listed in Table S2 in the supplemental material.

Statistical analysis. Statistical analyses were performed with Student's *t* test for comparison between two samples and analysis of variance with Bonferroni's *post hoc* test for multiple comparisons using GraphPad Prism software (GraphPad Software).

SUPPLEMENTAL MATERIAL

Supplemental material is available online only.

SUPPLEMENTAL FILE 1, PDF file, 0.1 MB.

ACKNOWLEDGMENTS

We thank Yuki Nakashima for technical support.

J.A.K., S.H., and Y.H. designed the experiments and wrote the manuscript. J.A.K. performed the experiments. T.S. supported the image analysis. C.K.S., H.I., J.M., K.A.-M., and H.N. critically read the manuscript and contributed to its preparation.

This work was funded by the Japan Society for the Promotion of Science (JSPS) (17K08624, 19H03414). J.A.K. and C.K.S. are supported by the MEXT scholarship.

We declare no competing interests.

REFERENCES

1. Allen NP, Donninger H, Vos MD, Eckfeld K, Hesson L, Gordon L, Birrer MJ, Latif F, Clark GJ. 2007. RASSF6 is a novel member of the RASSF family of tumor suppressors. Oncogene 26:6203–6211. https://doi.org/10.1038/sj.onc.1210440.

2. Ikeda M, Hirabayashi S, Fujiwara N, Mori H, Kawata A, Iida J, Bao Y, Sato Y, Iida T, Sugimura H, Hata Y. 2007. Ras-association domain family protein 6 induces apoptosis via both caspase-dependent and caspase-independent pathways. Exp Cell Res 313:1484–1495. https://doi.org/10.1016/j.yexcr.2007.02.013.
3. Iwasa H, Jiang X, Hata Y. 2015. RASSF6; the putative tumor suppressor of the RASSF family. Cancers (Basel) 7:2415–2426. https://doi.org/10.3390/cancers7040899.
4. Hesson LB, Dunwell TL, Cooper WN, Catchpoole D, Brini AT, Chiaramonte R, Griffiths M, Chalmers AD, Maher ER, Latif F. 2009. The novel RASSF6 and RASSF10 candidate tumour suppressor genes are frequently epigenetically inactivated in childhood leukaemias. Mol Cancer 8:42. https://doi.org/10.1186/1476-4598-8-42.
5. Richter AM, Pfeifer GP, Dammann RH. 2009. The RASSF proteins in cancer; from epigenetic silencing to functional characterization. Biochim Biophys Acta 1796:114–128. https://doi.org/10.1016/j.bbcan.2009.03.004.
6. Wen Y, Wang Q, Zhou C, Yan D, Qiu G, Yang C, Tang H, Peng Z. 2011. Decreased expression of RASSF6 is a novel independent prognostic marker of a worse outcome in gastric cancer patients after curative surgery. Ann Surg Oncol 18:3858–3867. https://doi.org/10.1245/s10434-011-1668-5.
7. Djos A, Martinsson T, Kogner P, Carén H. 2012. The RASSF gene family members RASSF5, RASSF6 and RASSF7 show frequent DNA methylation in neuroblastoma. Mol Cancer 11:40. https://doi.org/10.1186/1476-4598-11-40.
8. Liang YY, Chen MY, Hua YJ, Chen S, Zheng LS, Cao X, Peng LX, Xie P, Huang BJ, Sun R, Wang L, Xiang YQ, Guo X, Qian CN. 2014. Downregulation of Ras association domain family member 6 (RASSF6) underlies the treatment resistance of highly metastatic nasopharyngeal carcinoma cells. PLoS One 9:e100843. https://doi.org/10.1371/journal.pone.0100843.
9. Mezzanotte JJ, Hill V, Schmidt ML, Shinawi T, Tommasi S, Krex D, Schackert G, Pfeifer GP, Latif F, Clark GJ. 2014. RASSF6 exhibits promoter hypermethylation in metastatic melanoma and inhibits invasion in melanoma cells. Epigenetics 9:1496–1503. https://doi.org/10.4161/15592294.2014.983361.
10. Guo W, Dong Z, Guo Y, Shen S, Guo X, Kuang G, Yang Z. 2016. Decreased expression and frequent promoter hypermethylation of RASSF2 and RASSF6 correlate with malignant progression and poor prognosis of gastric cardia adenocarcinoma. Mol Carcinog 55:1655–1666. https://doi.org/10.1002/mc.22416.
11. Ye HL, Li DD, Lin Q, Zhou Y, Zhou QB, Zeng B, Fu ZQ, Gao WC, Liu YM, Chen RW, Li ZH, Chen RF. 2015. Low RASSF6 expression in pancreatic ductal adenocarcinoma is associated with poor survival. World J Gastroenterol 21:6621–6630. https://doi.org/10.3748/wjg.v21.i21.6621.
12. Tan S, Bian X, Wu B, Chen X. 2019. RASSF6 is downregulated in human bladder cancers and regulates doxorubicin sensitivity and mitochondrial membrane potential via the Hippo signaling pathway. Onco Targets Ther 12:9189–9200. https://doi.org/10.2147/OTT.S217041.
13. Younesian S, Shahkarami S, Ghaffari P, Alizadeh S, Mehrasa R, Ghaffari SH. 2019. Residual methylation of tumor suppressor gene promoters, RASSF6 and RASSF10, as novel biomarkers for minimal residual disease detection in adult acute lymphoblastic leukemia. Ann Hematol 98:2719–2727. https://doi.org/10.1007/s00277-019-03775-y.
14. Ikeda M, Kawata A, Nishikawa M, Tateishi Y, Yamaguchi M, Nakagawa K, Hirabayashi S, Bao Y, Hidaka S, Hirata Y, Hata Y. 2009. Hippo pathway-dependent and -independent roles of RASSF6. Sci Signal 2:ra59. https://doi.org/10.1126/scisignal.2000300.
15. Withanage K, Nakagawa K, Ikeda M, Kurihara H, Kudo T, Yang Z, Sakane A, Sasaki T, Hata Y. 2012. Expression of RASSF6 in kidney and the implication of RASSF6 and the Hippo pathway in the sorbitol-induced apoptosis in renal proximal tubular epithelial cells. J Biochem 152:111–119. https://doi.org/10.1093/jb/mvs056.
16. Iwasa H, Kudo T, Maimaiti S, Ikeda M, Maruyama J, Nakagawa K, Hata Y. 2013. The RASSF6 tumor suppressor protein regulates apoptosis and the cell cycle via MDM2 protein and p53 protein. J Biol Chem 288:30320–30329. https://doi.org/10.1074/jbc.M113.507384.
17. Sarkar A, Iwasa H, Hossain S, Xu X, Sawada T, Shimizu T, Maruyama J, Arimoto-Matsuzaki K, Hata Y. 2017. Domain analysis of Ras-association domain family member 6 upon interaction with MDM2. FEBS Lett 591:260–272. https://doi.org/10.1002/1873-3468.12551.
18. Shimizu T, Nakamura T, Inaba H, Iwasa H, Maruyama J, Arimoto-Matsuzaki K, Nakata T, Nishina H, Hata Y. 2020. The RAS-interacting chaperone UNC119 drives the RASSF6-MDM2-p53 axis and antagonizes RAS-mediated malignant transformation. J Biol Chem 295:11214–11230. https://doi.org/10.1074/jbc.RA120.012649.
19. Hossain S, Iwasa H, Sarkar A, Maruyama J, Arimoto-Matsuzaki K, Hata Y. 2018. The RASSF6 tumor suppressor protein regulates apoptosis and the cell cycle progression via retinoblastoma protein. Mol Cell Biol 38:e00046-18. https://doi.org/10.1128/MCB.00046-18.
20. Wang M, Gu C, Qi T, Tang W, Wang L, Wang S, Zeng X. 2007. BAF53 interacts with p53 and functions in p53-mediated p21-gene transcription. J Biochem 142:613–620. https://doi.org/10.1093/jb/mvm176.
21. Oh J, Sohn DH, Ko M, Chung H, Jeon SH, Seong RH. 2008. BAF60a interacts with p53 to recruit the SWI/SNF complex. J Biol Chem 283:11924–11934. https://doi.org/10.1074/jbc.M705401200.
22. Han J, Kim T, Moon S, Park J-H, Lee W, Ko Y-J, Ryu K-S, Yun J-H, Lee W. 2021. NMR spectroscopy uncovers direct interaction between BAF60A and p53. Biochem Biophys Res Commun 534:815–821. https://doi.org/10.1016/j.bbrc.2020.10.101.
23. Iwasa H, Kuroyanagi H, Maimaiti S, Ikeda M, Nakagawa K, Hata Y. 2013. Characterization of RSF-1, the Caenorhabditis elegans homolog of the Ras-association domain family protein 1. Exp Cell Res 319:1–11. https://doi.org/10.1016/j.yexcr.2012.10.008.
24. Zhao K, Wang W, Rando OJ, Xue Y, Swiderek K, Kuo A, Crabtree GR. 1998. Rapid and phosphoinositol-dependent binding of the SWI/SNF-like BAF complex to chromatin after T lymphocyte receptor signaling. Cell 95:625–636. https://doi.org/10.1016/S0092-8674(00)81633-5.
25. Van Duyne R, Guendel I, Narayanan A, Gregg E, Shafagati N, Tyagi M, Easley R, Klase Z, Nekhai S, Kehn-Hall K, Kashanchi F. 2011. Varying modulation of HIV-1 LTR activity by Baf complexes. J Mol Biol 411:581–596. https://doi.org/10.1016/j.jmb.2011.06.001.
26. Avruch J, Xavier R, Bardeesy N, Zhang XF, Praskova M, Zhou D, Xia F. 2009. Rassf family of tumor suppressor polypeptides. J Biol Chem 284:11001–11005. https://doi.org/10.1074/jbc.R800073200.
27. Sherwood V, Recino A, Jeffries A, Ward A, Chalmers AD. 2009. The N-terminal RASSF family: a new group of Ras-association-domain-containing proteins, with emerging links to cancer formation. Biochem J 425:303–311. https://doi.org/10.1042/BJ20091318.
28. Underhill-Day N, Hill V, Latif F. 2011. N-terminal RASSF family: RASSF7-RASSF10. Epigenetics 6:284–292. https://doi.org/10.4161/epi.6.3.14108.
29. Iwasa H, Hossain S, Hata Y. 2018. Tumor suppressor C-RASSF proteins. Cell Mol Life Sci 75:1773–1787. https://doi.org/10.1007/s00018-018-2756-5.
30. Reeves ME, Firek M, Chen ST, Amaar Y. 2013. The RASSF1 gene and the opposing effects of the RASSF1A and RASSF1C isoforms on cell proliferation and apoptosis. Mol Biol Int 2013:145096. https://doi.org/10.1155/2013/145096.
31. Vlahov N, Scrace S, Soto MS, Grawenda AM, Bradley L, Pankova D, Papaspyropoulos A, Yee KS, Buffa F, Goding CR, Timpson P, Sibson N, O'Neill E. 2015. Alternate RASSF1 transcripts control SRC activity, E-cadherin contacts, and YAP-mediated invasion. Curr Biol 25:3019–3034. https://doi.org/10.1016/j.cub.2015.09.072.
32. Xu X, Iwasa H, Hossain S, Sarkar A, Maruyama J, Arimoto-Matsuzaki K, Hata Y. 2017. BCL-XL binds and antagonizes RASSF6 tumor suppressor to suppress p53 expression. Genes Cells 22:993–1003. https://doi.org/10.1111/gtc.12541.
33. Iwasa H, Sarkar A, Shimizu T, Sawada T, Hossain S, Xu X, Maruyama J, Arimoto-Matsuzaki K, Withanage K, Nakagawa K, Kurihara H, Kuroyanagi H, Hata Y. 2018. UNC119 is a binding partner of tumor suppressor Ras-association domain family 6 and induces apoptosis and cell cycle arrest by MDM2 and p53. Cancer Sci 109:2767–2780. https://doi.org/10.1111/cas.13706.
34. Yu DS, Zhao R, Hsu EL, Cayer J, Ye F, Guo Y, Shyr Y, Cortez D. 2010. Cyclin-dependent kinase 9-cyclin K functions in the replication stress response. EMBO Rep 11:876–882. https://doi.org/10.1038/embor.2010.153.